Why Does Large Relative Humidity with Respect to Ice Persist in Cirrus Ice Clouds?

A. Bogdan*,†,‡ and M. J. Molina§

Department of Physics, P.O. Box 48, and Laboratory of Polymer Chemistry, Department of Chemistry, P.O. Box 55, University of Helsinki, FIN-00014 Helsinki, Finland, Institute of Physical Chemistry, University of Innsbruck, Innrain 52a, A-6020 Innsbruck, Austria, and Department of Chemistry and Biochemistry, University of California, San Diego, La Jolla, California 92093-0356

Received: July 6, 2009; Revised Manuscript Received: November 11, 2009

According to observations, a large relative humidity with respect to ice, $RH_i \gg 100\%$, often persists outside and inside upper tropospheric cirrus ice clouds. The persistence of the large in-cloud RH_i means that H_2O is slowly deposited onto cloud ice crystals. This unusual physical situation is similar to one in which a released body would slowly fall owing to gravitation. Here we present a physical mechanism which can be responsible for the persistence of large in-cloud RH_i. We find that clear-sky RH_i up to 176% can be built up prior to the formation of ice cirrus by the homogeneous freezing of aqueous droplets containing H_2SO_4 and HNO_3. As the droplets are cooled, a phase separation, which occurs during freezing, leads to the formation of a residual solution coating around the ice crystals formed. The coating can serve as a shield, slowing the rate of ice growth by $\sim 10^3$ in comparison with uncoated ice, and this can be a reason for the persistence of the large in-cloud RH_i.

1. Introduction

Upper tropospheric cirrus ice clouds are thought to limit the accumulation of water vapor in the upper troposphere (UT), because the growth and sedimentation of cirrus ice crystals redistribute moisture to lower levels. However, observations often reveal large and persistent moisture outside (in clear sky) and inside ice cirrus clouds[1−4] formed near the tropopause region in situ, i.e., not influenced by a deep convective water vapor source.[3] In the UT, water vapor is the dominant greenhouse gas. Therefore, it is important to know the nature of the processes underlying accumulation and persistence of large moisture in the UT. On the other hand, the knowledge of the critical values of humidity, at which cirrus ice clouds start developing, is important for the parametrization of cirrus and climate models.[5] Cirrus ice clouds, being globally widespread, are important climate regulators.

The UT moisture is equally expressed either as relative humidity with respect to water, RH_w, or as relative humidity with respect to ice, RH_i.[5] Since under atmospheric conditions liquid water does not exist below the homogeneous freezing temperature of $T_h \approx 233$ K,[6,7] the vapor pressure of liquid water is extrapolated to low temperatures. In this paper, we will use RH_i because the observed UT moisture data are usually expressed as RH_i.[1−4] In the UT, the observed clear-sky and in-cloud RH_i often exceeds 100% and below ∼195 K can reach as large as 200%.[1] The buildup of large RH_i, which is not influenced by a deep convective water vapor source, suggests that cirrus ice clouds are formed by homogeneous freezing of aqueous aerosol droplets. In the UT, the precursors of cirrus ice clouds can be pre-existing H_2SO_4/H_2O aerosol droplets.[8,9] The UT aerosol droplets can also contain HNO_3.[4] In the UT, H_2SO_4 and HNO_3 are of natural and anthropogenic origin: descending stratospheric H_2SO_4/H_2O aerosol,[10] volcanic eruptions,[11] burning of sulfur-containing fossil fuels,[12] nitrogen-based fertilizer, vegetation, oceanic sources,[13,14] etc.

The buildup of the upper tropospheric $RH_i \gg 100\%$ prior to the onset of the formation of cirrus ice clouds has been studied theoretically[15−17] and experimentally.[9,18,19] The experimental studies showed that before cirrus ice clouds start developing the clear-sky RH_i may reach up to ∼170%.[18] The recent generalizations of classical ice nucleation theory indicate that RH_i as large as 180−200% may be required for the initiation of the homogeneous freezing of haze droplets with a diameter of 0.05−5 μm.[5] However, in this paper we will not consider the mechanisms of the formation of large clear-sky RH_i. A goal of this paper is to present a physical mechanism which can be responsible for the persistence of in-cloud $RH_i \gg 100\%$.

According to the calculations of some authors, numerous cirrus ice crystals, which are formed by homogeneous freezing of aqueous droplets, would rapidly consume water vapor and lower the elevated in-cloud moisture to $RH_i \approx 100\%$.[20,21] However, there is evidence that the deposition of water vapor on cirrus ice crystals is far from instantaneous.[17,22] The deposition of water vapor is determined by the "phase relaxation time" expressed as $\tau = (4\pi D N_i r_i)^{-1}$, where D is the H_2O diffusion coefficient, N_i the ice crystal concentration, and r_i the crystal radius. τ can vary from ∼0.5 to 2 h.[22] Even after 1 h of cirrus cloud development, RH_i was calculated to remain at 105−110%[22] or even larger than 130%.[17] To explain the large in-cloud RH_i, a hypothesis was made; it suggested that the deposition coefficient of H_2O for small ice crystals may be <0.01,[23] which would prolong the in-cloud RH_i near the critical value for ice nucleation. Subsequent works disputed[24] and confirmed[25] the hypothesis. However, the confirmation for the small deposition coefficient was reported only for ice crystals at ∼223 K[25] whereas large RH_i up to 200% is usually observed below ∼195 K.[1] Further, the International Cirrus Parcel Model Comparison Project, CPMCP, considered the deposition coefficients of H_2O on the order of 0.1−1.[26] In the simulation aimed to explain in-cloud $RH_i \approx 180\%$, which was observed during

† Departments of Physics and Chemistry, University of Helsinki.
‡ University of Innsbruck (present address).
§ University of California, San Diego.

10.1021/jp9063609
Published on Web 11/19/2009

the CRYSTAL-FACE field campaign on July 13, 2002, over Florida, the deposition coefficient was assumed to be smaller than 0.03.[17] However, the reason for such a small deposition coefficient was unclear. The proposed explanation for the in-cloud $RH_i \approx 130\%$ by the formation of a new class of HNO_3-containing ice particles, so-called Δ-ice,[4] was shown to violate the second law of thermodynamics.[27] There is also an opinion that cubic ice may considerably contribute to the large RH_i.[28] The cubic form of ice is metastable with respect to the stable hexagonal form of ice, which is usually formed under atmospheric conditions. Some authors believe that the vapor pressure of cubic ice is ∼10% larger than that of hexagonal ice[28] and consequently may account for ∼10% of the observed elevated RH_i. However, the most recent estimation of the enthalpy change of the cubic-to-hexagonal ice transition suggests that the vapor pressure difference between cubic and hexagonal ice may be less than 1%.[29]

In this paper, we present the results of the study of the low-temperature phase transitions of emulsified micrometer-scaled H_2SO_4/H_2O and $H_2SO_4/HNO_3/H_2O$ droplets of sizes and compositions representative of the UT. Our experimental and computational results demonstrate that other physical processes can be responsible for the maintenance of in-cloud $RH_i \gg 100\%$. These involve the effects of H^+, SO_4^{2-}, and NO_3^-on homogeneous ice crystal nucleation and the formation of a residual solution coating around the ice crystals in cirrus ice clouds formed by the homogeneous freezing of aqueous aerosol droplets.

2. Experimental Section

2.1. Materials and Methods. We studied micrometer-scaled H_2SO_4/H_2O droplets with a composition of 5−30 wt % H_2SO_4 and $H_2SO_4/HNO_3/H_2O$ droplets with a composition of 5−25 wt % H_2SO_4 and 1−7 wt % HNO_3 by using differential scanning calorimetry (DSC). The droplets were prepared by emulsifying bulk solutions of the corresponding compositions. The bulk solutions were prepared by mixing the calculated amount of 95−97 wt % H_2SO_4 and 65 wt % HNO_3 (Riedel-de Haën, Germany) with the corresponding amount of ultrapure deionized water. The accuracy of the method of solution preparation was verified by the titration of H_2SO_4/H_2O and HNO_3/H_2O against standard 2 N NaOH. The titration showed an accuracy of ±0.1 wt %. The advantage of using emulsion and DSC techniques is that they allow performing measurements in which three parameters such as the size and composition of emulsified droplets and the cooling rate are similar to those encountered in the atmosphere.

2.2. Emulsification Procedure. The oil phase, which was used for the preparation of emulsions, was prepared by using halocarbon 0.8 oil (Halocarbon Producs Corp.) and lanolin (Sigma-Aldrich). The halocarbon oil is a low molecular weight polymer of chlorotrifluoroethylene (PCTFE) and is chemically inert to practically all acids, alkalis, and oxidizing agents. Lanolin is a natural organic substance which consists of cholesterol, wool alcohols, and the esters derived from several fatty acids. Lanolin is insoluble in water but makes an emulsion.

The solution-in-oil emulsions were prepared according to the emulsion technique described elsewhere.[30] In short, the oil phase was prepared by mixing 80 wt % halocarbon 0.8 oil and 20 wt % lanolin. The solution/oil mixtures of 1/10 by volume were shaken for 5−8 min with a high-speed shaker (Thermolyne Maxi-Mix) at 1400−2000 rpm. The diameter of the droplets was measured with an optical microscope. In the emulsions, the diameter of the droplets was <5 μm. The stability of the emulsions depends on the solution composition. Some emulsions are stable for several days, others for more than several months.

2.3. DSC Measurements. We measured the emulsified solutions using a Mettler Toledo DSC 822 calorimeter. The device was well calibrated and reproduced the melting points of indium (429.75 K), water (273.15 K), and heptane (∼182 K) with an accuracy of ±0.3 K. The measurements were performed at a scanning rate of 3 K/min (180 K/h), which is much larger than the atmospheric cooling rates of 2−80 K/h.[31] However, previous work showed that the reduction of the cooling rate from 5 K/min (300 K/h) to 0.1 K/min (6 K/h) lowers the freezing temperature of ice by less than 1−2 K.[30] The recent generalizations of classical nucleation theory also indicate that the significant jump in the freezing temperature of ice occurs when the fall of the cooling rate is several orders of magnitude.[5] Therefore, the choice of a cooling rate of 3 K/min can be considered as a reasonable approximation of the atmospheric cooling rates for measuring the *freezing* temperature of aqueous droplets relevant for the atmosphere. The mass of the emulsion samples was between ∼20 and 35 mg. The emulsion samples were cold sealed in a standard Al crucible with a volume of 40 μL. Since the number of droplets in the DSC samples is $\sim>10^5$, the obtained results are of statistical significance.[30] Numerous repetitive measurements were made to verify the reproducibility of the results.

Since the halocarbon 0.8 oil is chemically inert, there is no reaction between the oil and solutions. The estimation of the stability of lanolin showed that there was no appreciable reaction between lanolin and concentrated H_2SO_4/H_2O and HNO_3/H_2O on the time scale of 2 days.[30] Nevertheless, to prevent any degradation of lanolin, all DSC measurements were performed within less than 2 h from the moment of contact between the solution and the oil phase.

3. Results and Discussion

3.1. Solution-Coated Ice Crystals. Recently we reported that cold ice cirrus clouds formed by homogeneous freezing H_2SO_4/H_2O droplets can consist of mixed-phase particles: an ice core + a H_2SO_4/H_2O coating.[8] Figure 1 presents an example of DSC thermograms which demonstrate that the freezing of $H_2SO_4/HNO_3/H_2O$ droplets with an excess of H_2SO_4 may also produce mixed-phase particles. The $H_2SO_4/HNO_3/H_2O$ droplets with an excess of H_2SO_4 are chosen because observations reveal a HNO_3 mixing ratio of almost zero in ice cirrus over the western Indian Ocean[32] to 1000 pptv in cirrus and contrails over southern Florida.[4] The thermograms similar to those presented in Figure 1 are also obtained from H_2SO_4/H_2O and $H_2SO_4/HNO_3/H_2O$ droplets in which $[H_2SO_4]$ varies between 5 and 25 wt % and $[HNO_3]$ is 1,2,3, 5, and 7 wt %. In Figure 1, the cooling and warming thermograms contain two exothermic-freezing and two endothermic-melting events, respectively. The warm exothermic and endothermic events, which produce a single transition peak, are due to the freezing out and melting of pure ice. The cold exothermic and endothermic events, which produce double or/and broad transition peaks, are due to the freezing and melting of a residual solution[8,33] which is formed by expelling H^+, SO_4^{2-}, and NO_3^- ions from the ice lattice during the nucleation and growth of ice. The order of the freezing events in H_2SO_4/H_2O and $H_2SO_4/HNO_3/H_2O$, i.e., which solid is formed first on cooling, is determined from the measurements in which the cooling of droplets is terminated immediately after the first freezing event. In this case, one obtains truncated thermograms which contain only warm freezing and melting peaks. From the fact that the temperature of the melting peak exactly matches

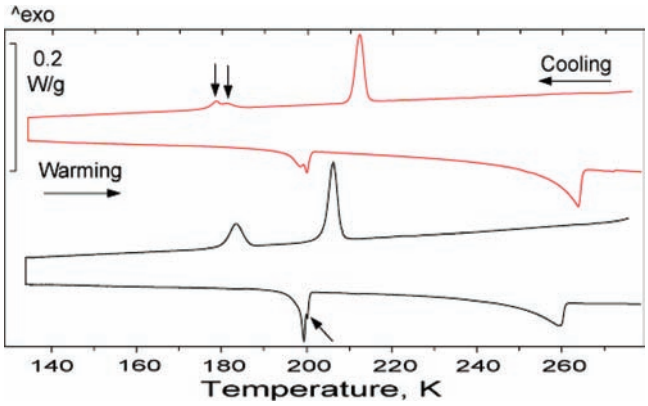

Figure 1. Typical calorimetric thermograms which demonstrate a phase separation into pure ice and a residual solution during the freezing of H_2SO_4/H_2O and H_2SO_4/ HNO_3/H_2O droplets (>10^5). The upper red cooling and warming thermograms are obtained from the emulsified droplets with a composition of 17 wt % H_2SO_4. The lower black thermograms are obtained from the emulsified droplets with a composition of 17 wt %/3 wt % H_2SO_4/HNO_3. In both emulsion samples, the warm exothermic/endothermic events are due to the freezing/melting of pure ice. In the upper red cooling thermogram, the two vertical arrows show the exothermal peaks of the formation of SAO and ice/SAT during the freezing of a residual solution. On warming, the ice/SAT and SAO melt at ~199.3 and ~200.3 K, respectively.[35] In the lower black cooling thermogram, the two freezing peaks, which are formed during the freezing of the residual solution, are overlapped (see the text). In the warming black thermogram, the tilted arrow shows the endothermic peak of the melting of SAO. The horizontal arrows show the direction of the temperature change of 3 K/min. The mass of the emulsion samples of binary and ternary solutions is 24.28 and 20.08 mg, respectively. The scaled bars denote heat flow through the samples.

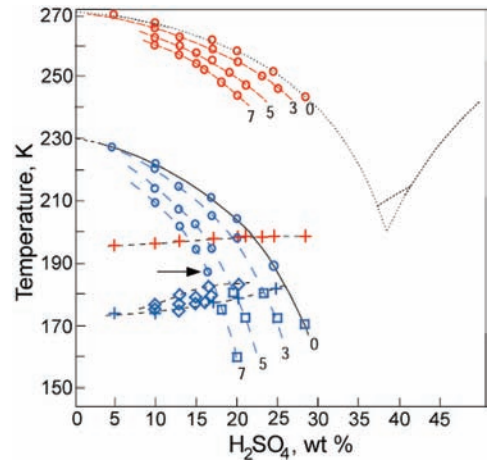

Figure 2. Experimental temperatures of the phase transformations of H_2SO_4/H_2O and $H_2SO_4/HNO_3/H_2O$ droplets. Numbers depict the HNO_3 concentration (wt %) in the $H_2SO_4/HNO_3/H_2O$ droplets. The dotted line is the equilibrium phase diagram of H_2SO_4/H_2O.[34,35] The blue circles are the peak freezing temperatures, T_i, and the red circles the melting temperatures, T_m, of pure ice. The blue plus signs are the peak freezing temperatures of the residual solution[8,33] with a composition of ~38 wt % H_2SO_4.[35] The blue tilted squares are the peak freezing temperatures of residual $H_2SO_4/HNO_3/H_2O$. The warmer freezing temperature of the residual solution corresponds to the larger amount of HNO_3 in the droplets. The blue squares are the peak temperatures of the complete freezing of the droplets, i.e., the temperatures at which the freezing of the pure ice and the residual solution overlap. The red plus signs are the eutectic melting points of the ice/hydrate mixture. For simplicity, the separate freezing and melting points of SAO and the eutectic mixture of ice/SAT[35] are not shown because they either are very close to each other or may overlap (see Figure 1).

the melting point of ice in the H_2SO_4/H_2O phase diagram,[34,35] one can infer that the warm transition peaks are due to the freezing and melting of pure ice. The remaining cold transition peaks are due to the freezing and melting of the residual H_2SO_4/H_2O solution. In the truncated thermograms obtained from $H_2SO_4/HNO_3/H_2O$ droplets, the temperature of the warm melting peak is slightly lower than the melting points of ice in the H_2SO_4/H_2O phase diagram because of the presence of HNO_3.[30,36]

The transition temperatures of $H_2SO_4/HNO_3/H_2O$ droplets, in which the amount of HNO_3 varies from 0 to 7 wt %, are shown in Figure 2. It is seen that the lowering of the freezing and melting temperatures of ice of $H_2SO_4/HNO_3/H_2O$ droplets in comparison with that of H_2SO_4/H_2O droplets increases with increasing HNO_3. It is also seen that although the freezing temperature of the ternary $H_2SO_4/HNO_3/H_2O$ residual solution increases with increasing of HNO_3 (blue tilted squares), it nevertheless always remains below the lowest atmospheric temperature of ~185 K. The complete freezing of H_2SO_4/H_2O and $H_2SO_4/HNO_3/H_2O$ droplets occurs below 180 K (blue squares). In the temperature regions between the two freezing events and between the two melting events, the particles are in the mixed-phase state: a pure ice core + a residual solution.

Figure 1 shows that the cold transition peaks are double or broad, which indicates that two solids are formed during the freezing of the residual solution. The double peaks are due to the formation and melting of sulfuric acid octahydrate ($H_2SO_4 \cdot 8H_2O$, SAO) and a eutectic mixture of ice/SAT (sulfuric acid tetrahydrate, $H_2SO_4 \cdot 4H_2O$).[35] In the cooling thermogram obtained from the 17 wt %/3 wt % H_2SO_4/HNO_3 droplets, the freezing peaks of SAO and ice/SAT overlap and produce one broad transition peak. The overlapping of the two freezing peaks may be brought about by the presence of 3 wt % HNO_3. The comparison of the cold double melting peaks reveals that the addition of HNO_3 changes the ratio of the areas of the melting peaks of SAO and ice/SAT. In the warming thermogram of ternary 17 wt %/3 wt % H_2SO_4/HNO_3 droplets, the area of the melting peak at ~199.3 K, which characterizes the melting of ice/SAT,[35] becomes larger, whereas the area of the melting peak at ~200.3 K, which characterizes the melting of SAO,[35] becomes smaller in comparison with the area of the corresponding peaks in the warming thermogram of 17 wt % H_2SO_4 droplets. The change of the ratio of the areas of the melting peaks indicates the redistribution of the amount of ice/SAT and SAO formed after the addition of HNO_3. In the DSC method, the area under the transition peak is proportional to the change of enthalpy in the material undergoing the phase transition and, consequently, proportional to the amount of the material undergoing the phase transition. The change of the ratio of the area of the melting peaks is also observed in the warming thermograms obtained from the ternary droplets of other studied compositions. However, the addition of 3 wt % HNO_3 to H_2SO_4/H_2O does not lead to the formation of the eutectic solid mixture of ice/NAT (nitric acid trihydrate, $HNO_3 \cdot 3H_2O$) which melts at ~220 K.[36,37] The eutectic melting point of ~220 K can be determined from Figure 4 of ref 36. It can also be determined if one plots the concentration of 17 wt %/3 wt % H_2SO_4/HNO_3 in Figure 2 of ref 36 and uses the lever rule. The absence of the melting peak at ~220 K indicates the absence of the eutectic solid mixture of ice/NAT. More about the $H_2SO_4/HNO_3/H_2O$ system and thorough references can be found elsewhere.[30,36,37]

3.2. Composition of the Residual H_2SO_4/H_2O Solution. For the calculation of the thickness of the solution coating around cirrus ice crystals and the impact of the coating on the rate of ice growth, one needs to know the composition of the coating or residual solution. The estimation of the composition of the residual solution is given below for H_2SO_4/H_2O droplets. In a

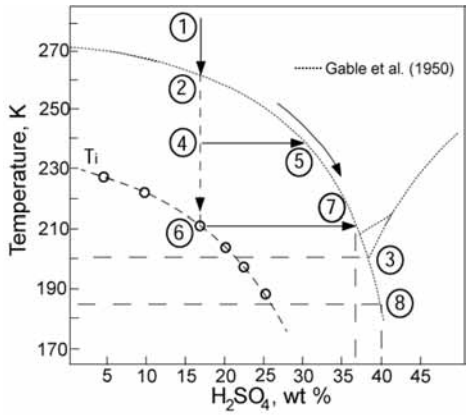

Figure 3. Freezing of bulk and emulsified H_2SO_4/H_2O. The bulk solution at point 1 is first cooled to point 2, where pure ice crystals begin to form. During further cooling, the ice crystals grow and the concentration of the residual solution increases along the ice/liquid equilibrium line until the eutectic concentration at point 3 is reached. The cooling below point 3 results in the formation of a solid mixture of pure ice and SAT. Points 4 and 5 denote the supercooling of the bulk solution and the corresponding concentration of the residual solution, respectively (see the text). The emulsified 17 wt % H_2SO_4 droplets are cooled to point 6, which is the peak temperature of the freezing out of pure ice in Figure 1. Point 7 is the concentration of the residual solution which corresponds to freezing point 6. Point 8 is the concentration of the residual solution which would be produced by emulsified ~26 wt % H_2SO_4 droplets which freeze at the lowest atmospheric temperature of ~185 K. The circles are the temperatures of the freezing out of pure ice from Figure 2. The arrows show the direction of the cooling of bulk and emulsified H_2SO_4/H_2O and the increase of the concentration of the residual solution.

similar way the composition of the residual solution can be estimated for $H_2SO_4/HNO_3/H_2O$ droplets. Figure 3 presents a partial phase diagram of H_2SO_4/H_2O,[34,35] the experimental freezing data of emulsified H_2SO_4/H_2O droplets from Figure 2, and a scheme of the freezing of bulk and emulsified H_2SO_4/H_2O. As an example we will consider the solution with a composition of 17 wt % H_2SO_4. According to the binary phase diagram, when a large volume of solution at point 1 is first cooled to point 2, pure ice crystals start forming. In the large volume of liquid, the walls of a container and/or suspended impurity particles can trigger heterogeneous freezing out of pure ice at a temperature corresponding to point 2 on the ice/solution equilibrium line. On further cooling, the ice crystals grow and the concentration of the solution increases along the ice/solution equilibrium line until the eutectic concentration of ~38 wt % H_2SO_4 is reached at ~200 K[34,35] (point 3 in Figure 3). Reducing the volume of the solution and/or increasing its purity, the bulk solution can be supercooled below the ice/solution equilibrium line, for example, to point 4. At this temperature the freezing out of pure ice leads to the formation of the residual solution with a concentration corresponding to point 5. On further cooling, the concentration of the residual solution increases along the ice/solution equilibrium line to point 3. It should be noticed that during the cooling of bulk seawater the concentration of the residual solution (which in the case of salt solutions is called freeze-concentrated brine) also increases with decreasing temperature.[38]

In cooled emulsified H_2SO_4/H_2O droplets, pure ice freezes out along the freezing line of T_i, which is depicted by circles connected by a dashed line in Figure 3. According to Figure 3, the concentration of the residual solution, which is formed after the freezing out of pure ice in the emulsified droplets with concentrations of 5−26 wt % H_2SO_4/H_2O, is between ~33 and

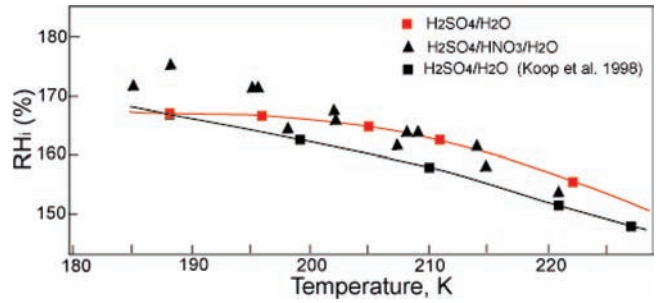

Figure 4. Clear-sky RH_i which would exist in the UT immediately prier to the formation of ice cirrus clouds by homogeneous freezing of H_2SO_4/H_2O and $H_2SO_4/HNO_3/H_2O$ droplets. The calculation of RH_i has been performed using the measured freezing temperatures of ice, T_i, from Figure 2 and the thermodynamic model[39] of the system $H^+-NH_4^+-SO_4^{2-}-NO_3^--H_2O$. The largest value of $RH_i \approx 176\%$ was calculated using T_i and the composition shown by the arrow in Figure 2.

40 wt % H_2SO_4. In the droplets with a composition of 17 wt % H_2SO_4, which freeze at $T_i \approx 211$ K (point 6), the concentration of the residual solution is ~36.5 wt % H_2SO_4 (point 7). In the droplets with a concentration of ~21 wt % H_2SO_4, pure ice freezes out at ~200 K, which leads to the formation of the residual solution with a eutectic concentration of ~38 wt % H_2SO_4.[34,35] At the lowest atmospheric temperature of ~185 K, the freezing out of pure ice in the droplets with a concentration of ~26 wt % H_2SO_4 would produce the residual solution with a concentration of ~40 wt % H_2SO_4 (point 8), which is on the extension of the ice/solution equilibrium line. In the temperature region of the existence of cold cirrus ice clouds, $T <$ ~210K, the concentration of the residual solution would be ~37−40 wt % H_2SO_4 (Figure 3). Because of the small variation of the concentration, for the calculation of the initial thickness of the H_2SO_4/H_2O coating around cirrus ice crystals, we will not use the temperature dependence of the concentration of the residual solution. As an initial concentration of the residual solution, we will take the eutectic concentration of 38 wt % H_2SO_4.

3.3. Clear-Sky RH_i Prior to the Formation of Cold Cirrus. In the absence of any deep convective water vapor sources, the temperature of the homogeneous freezing of UT aqueous aerosol droplets will determine the highest clear-sky RH_i. Assuming that the UT aerosol droplets have a composition similar to that of the laboratory droplets, we calculated the RH_i which would exist immediately prior to the formation of cirrus ice clouds. The calculations were performed by using the measured freezing temperatures of ice, T_i, as collected in Figure 2, and the thermodynamic model of the system $H^+-NH_4^+-SO_4^{2-}-NO_3^--H_2O$.[39] The results of the calculations are shown in Figure 4. Also shown are the RH_i data which were calculated by using the freezing temperatures of H_2SO_4/H_2O droplets from ref 9 (black line). Our values of RH_i calculated for H_2SO_4/H_2O droplets are slightly larger than those which were calculated by using the freezing data from ref 9. The difference can be accounted for by the fact that, in our measurements, the diameter of the H_2SO_4/H_2O droplets is <5 μm, whereas in ref 9 it is between ~3.1 and ~12.6 μm. The smaller the size of the droplets, the colder the freezing temperature T_i and consequently the larger the RH_i. At the temperature of ~188 K our calculated value of RH_i is similar to that calculated by using the freezing data from ref 9.

Figure 4 shows that the calculated values of the clear-sky RH_i increase with decreasing temperature both for H_2SO_4/H_2O and for $H_2SO_4/HNO_3/H_2O$ droplets and can reach ~176%. Although the value of $RH_i \approx 176\%$ is about 25% smaller than the largest RH_i recently observed below ~195 K,[1] it nevertheless

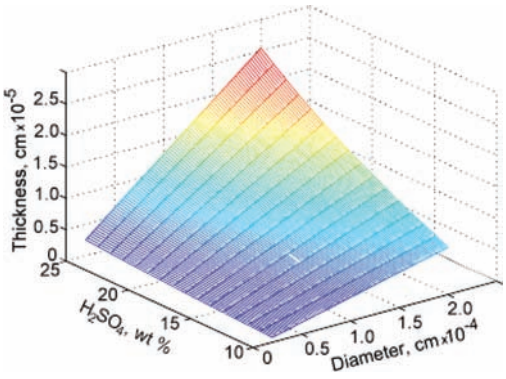

Figure 5. Thickness of the coating with a composition of 38 wt % H_2SO_4 which would envelop spherical ice crystals after the freezing of H_2SO_4/H_2O droplets. The thickness of the coating was calculated for the droplets with a diameter of 0.2−2 μm and a composition of 10−25 wt % H_2SO_4.

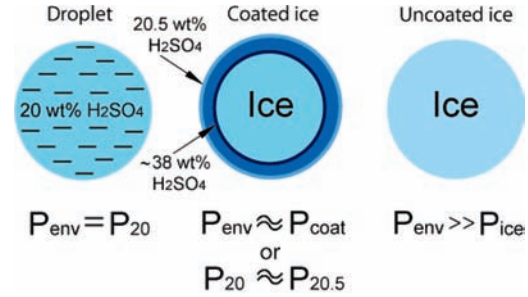

Figure 6. Vapor pressures of an aqueous droplet and coated and uncoated ice crystals. As an example, the coated ice crystal is assumed to be formed after the freezing out of ice in a 20 wt % H_2SO_4 droplet. P_{env} is the environmental water vapor pressure, which (in this particular case) is the same as the water pressure, P_{20}, of a freezing 20 wt % H_2SO_4 droplet. P_{coat} is the water pressure of the coating. P_{coat} is similar to the water pressure of the outer side of the coating of 20.5 wt % H_2SO_4. P_{ice} is the water pressure of a pure ice crystal. The arrows show the concentrations of the inner and outer sides of the coating (see the text for details).

is ∼10% larger than the RH_i predicted by previous laboratory work.[9] Our calculated values of RH_i are also in good agreement with recent calculations performed by using the formulas of the generalizations of classical ice nucleation theory which predict $RH_i > 170\%$.[5]

Normally, it is thought that cirrus ice clouds consist of pure ice crystals. If this is the case, then the time needed to consume elevated in-cloud moisture ($RH_i \gg 100\%$) due to the deposition of H_2O on ice crystals would be ∼1 min.[21] Taking into account the "phase relaxation time", in-cloud $RH_i > 100\%$ may persist for about 2 h.[22] However, in situ observations often reveal persistent in-cloud $RH_i \gg 100\%$.[1−4] The physical mechanism, which can account for the persistence of in-cloud $RH_i \gg 100\%$, is presented in the next section.

3.4. Impact of a Coating on the Rate of Ice Growth. The calculations of the thickness of the coating around cirrus ice crystals and the impact of the coating on the rate of ice growth, and consequently on the rate of the consumption of moisture, are given below for H_2SO_4/H_2O droplets. The H_2SO_4/H_2O system has been well studied, and its thermodynamic data are well documented.[34,35,44,47] At first we calculate the thickness of the coating which is formed immediately after the freezing out of pure ice in H_2SO_4/H_2O droplets. According to the discussion in section 3.2, for the calculation of the initial thickness of the residual solution, we will use the eutectic concentration of 38 wt % H_2SO_4. Figure 5 presents the calculated thickness for the coating with a composition of 38 wt % H_2SO_4[34,35] which would envelop spherical ice crystals formed after the freezing of the droplets with a diameter of 0.2−2 μm and composition of 10−25 wt % H_2SO_4. The UT droplets can reach a diameter of ∼2 μm,[8,10] and Figure 2 demonstrates that the droplets with a concentration of >∼25 wt % H_2SO_4 freeze below the lowest atmospheric temperature of ∼185 K. The assumption for the spherical ice crystals is justified by two facts: (i) The observations show that small cirrus ice crystals are quasi-spherical.[2,3,40] (ii) Slurry ice,[41] which is formed during the cooling of concentrated solutions, consists of small spherical ice crystals. For the simplicity of the calculations, we assumed that the surface of spherical ice crystals is smooth. Figure 5 shows that the thickness of the initial coating may be between ∼8 and 255 nm. We also calculate the thickness of the *aged* coating which would envelop the ice crystals with a diameter of 10 μm. In situ observations of cold cirrus showed that ice crystals are smaller than ∼10−12 μm.[42] We assume that the composition of the aged coating is the average of 38 wt % H_2SO_4 and the equilibrium concentration of freezing droplets. The calculations show that if the ice crystals originate from the droplets with a diameter of 0.8−2 μm and composition of 10−25 wt % H_2SO_4, then the aged coating would be ∼0.5−11 nm thick.

In the UT, the growth rate of coated ice crystals will differ from that of uncoated ones since the coating can serve as a "shield" reducing the flux of H_2O molecules to the ice surface. Figure 6 demonstrates a difference between the physical mechanisms of the growth of coated and uncoated ice crystals. The uncoated ice crystals experience rapid growth due to fast deposition of H_2O *directly* on the ice surface. In the case of coated ice, H_2O molecules first condense on the coating, dilute it, diffuse to the ice core, and only then become incorporated into the ice lattice. The condensation−dilution process is due to the fact that the water pressure of 38 wt % H_2SO_4 is lower than the environmental water pressure, which is similar to that of the freezing H_2SO_4/H_2O droplets. The diffusion of H_2O through the coating is due to the concentration gradient between the inner and outer sides of the coating (Figure 6). The inner side of the coating, which is in contact with an ice core, is in equilibrium with the ice and therefore possesses a composition of ∼38 wt % H_2SO_4. The outer side of the coating, which is exposed to the environmental gaseous phase, would rapidly acquire the composition of the freezing droplets to equilibrate with the environmental water vapor. We assume that one monolayer of the outer side of the coating (∼0.3 nm) will govern the flux of the condensing H_2O. We calculate the equilibration time to be ≤0.0013 s (Figure 7a). This time is in good agreement with the earlier calculation for the equilibration time of the H_2SO_4/H_2O aerosol.[43,44] Of course, speaking about one monolayer of the outer side of the coating, we assume that the thickness of the coating is larger than several monolayers. If the coating is less than one monolayer thick, which will happen when an ice core grows to a sufficiently large diameter, then the growth of ice will be governed by the direct deposition of H_2O onto the pure ice surface.

As the outer side of the coating has equilibrated with the environment, the flux of condensing H_2O is now reduced to zero, since the amounts of the condensing and evaporating H_2O at equilibrium are equal. Due to the aforementioned concentration gradient, the surface H_2O molecules diffuse to the ice core. This diffusion of H_2O increases the concentration of the outer side of the coating—which in turn makes H_2O condense to restore the equilibrium. Since the water pressure of the coating is much higher than that of the ice, the flux of H_2O condensing

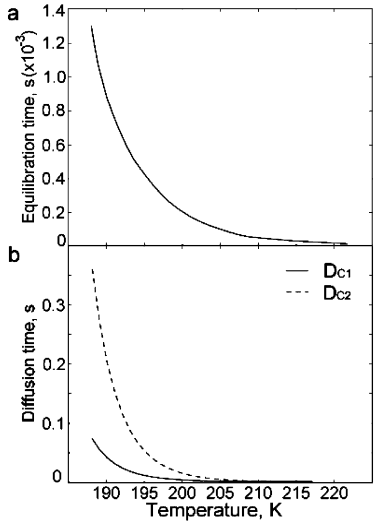

Figure 7. Equilibration and diffusion times: (a) time needed for the outer side of the coating to equilibrate from the initial concentration of 38 wt % H_2SO_4 to the concentration of H_2SO_4/H_2O droplets for which the freezing temperatures are shown in Figure 2, (b) time needed for a HCl molecule to diffuse through the coating with a composition of 38 wt % H_2SO_4 and thickness of 8−255 nm (Figure 5). The calculation of the diffusion times was performed for the two diffusion coefficients D_{C_1} and D_{C_2} (see the text for details).

on the coating is much smaller than that which is deposited on the pure ice surface. To calculate these fluxes, we used the continuum regime of ice growth, since for the UT pressure of 100−200 mbar the mean free path of an air molecule is ∼0.4−0.2 μm, i.e., smaller than the diameter of young ice crystals, which we assume to be 0.5−10 μm. The flux of H_2O condensed onto the coating is proportional to $\Delta_{coat} = n_{env} - n_{coat}$,[45,46] where n_{env} is the number concentration of H_2O in the environmental vapor and n_{coat} is that of H_2O above the coating. The flux of H_2O deposited on the pure ice is proportional to $\Delta_{ice} = n_{env} - n_{ice}$, where n_{ice} is the number concentration of H_2O above the ice. Number concentrations were calculated from the formula $p = nkT_i$, where T_i is the freezing temperature of ice from Figure 2, p is the corresponding water pressure, and k is the Boltzmann constant. Since $\Delta_{coat} \ll \Delta_{ice}$ and the inequality increases with decreasing temperature, the flux of H_2O condensed on the coating is much smaller than that which is deposited on the pure ice surface.

3.5. Growth of a Coated Ice Crystal. From the discussion above, the flux of H_2O condensed on a coating depends on the difference between the concentration of the outer side of the coating and the equilibrium concentration of freezing droplets. Figure 6, in which the water vapor pressures of a mother solution droplet and coated and uncoated ice crystals are presented, demonstrates why the flux of H_2O condensed on the coating depends on the concentration difference. As an example, the water pressure of a coated ice crystal formed after the freezing of a 20 wt % H_2SO_4 droplet is considered. Before freezing, the droplet is in equilibrium with the environmental water pressure, i.e., $p_{env} = p_{20}$. After freezing, the outer side of the coating rapidly equilibrates to the equilibrium freezing concentration of 20 wt % H_2SO_4. Due to the concentration gradient between the inner and outer sides of the coating, the surface H_2O molecules start diffusing to the ice core. The outflow of H_2O from the surface layer will increase the concentration of the outer side of the coating, for example, to 20.5 wt % H_2SO_4 (Figure 6). In this case the concentration difference of 0.5 wt % H_2SO_4 will govern the flux of H_2O condensed on the coating

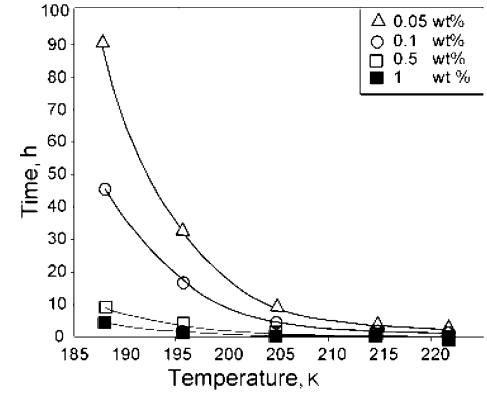

Figure 8. Time (h) needed for a coated ice crystal to grow from a diameter of 0.25 μm to a diameter of 10 μm. The symbols indicate the difference between the concentration of the outer surface of the coating and the equilibrium concentration of the freezing H_2SO_4/H_2O droplets (see the text for details).

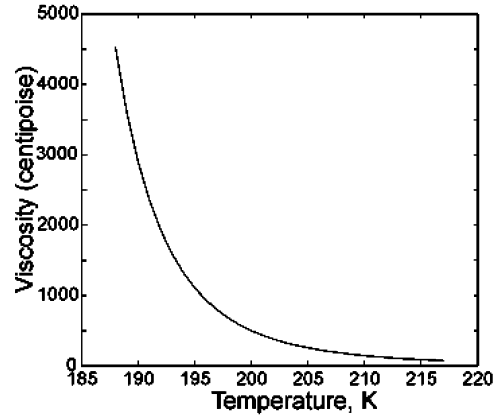

Figure 9. Viscosity of 38 wt % H_2SO_4 as a function of temperature. The viscosity was calculated according to Williams and Long.[47]

through the difference of $\Delta_{coat} = n_{env} - n_{20.5}$[45,46] $= n_{20} - n_{20.5}$, where $n_{env} = n_{20}$ because $p_{env} = p_{20}$. This relation indicates that the smaller the concentration difference, the smaller the flux of H_2O condensed on the coating. Of course, in the UT, the difference between the concentration of the outer side of the coating and the equilibrium concentration may change due to the change of temperature and environmental humidity, which will change the flux of condensing H_2O.

Assuming the accommodation coefficient of condensing H_2O molecules to be 1, we calculated the time needed for a coated ice crystal to grow from a diameter of $d_i = 0.25$ μm to $d_f = 10$ μm at the UT pressure of 200 mbar. Since the exact concentration difference is not known, we perform sensitivity calculations for the four different concentration differences; i.e., we assume that the concentration of the outer side of the coating exceeds the equilibrium concentration by 0.05, 0.1, 0.5, and 1 wt % H_2SO_4. The results of the calculations presented in Figure 8 indicate that indeed the time of ice growth strongly depends on the concentration difference. Insight into the concentration difference can be obtained from a comparison of the equilibration time (Figure 7a) and the time needed for H_2O to diffuse through the coating (Figure 7b). We calculate the latter using the available viscosity data of H_2SO_4/H_2O.[47] First, the viscosity η of 38 wt % H_2SO_4 as a function of temperature was calculated. The result of the calculation is presented in Figure 9. It is seen that the viscosity of the 38 wt % H_2SO_4 solution steeply increases with decreasing temperature. Using the calculated viscosity data, the diffusion coefficient of $D(T)$ was then

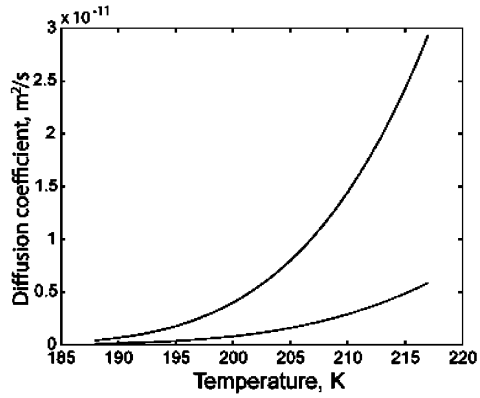

Figure 10. Two diffusion coefficients for HCl in 38 wt % H_2SO_4 solution as a function of temperature. The diffusion coefficients were calculated using the Stokes−Einstein formula of $D = C(T/\eta)$ for two different constants, C_1 and C_2 (see the text for details).

calculated using the Stokes−Einstein relation of $D = C(T/\eta)$ for two different constants, $C_1 = 10^{-7}$ and $C_2 = C_1/5$ [(cm² cP)/(s K)], which are in fact for HCl in H_2SO_4.[44,47] The actual value of C for H_2O in H_2SO_4 is not known. The results of the calculation are shown in Figure 10. Using the two diffusion coefficients, $D_{C_1}(T)$ and $D_{C_2}(T)$, we calculate the diffusion times $t_{D_{C1}}(T)$ and $t_{D_{C2}}(T)$ as a function of temperature. The results of the calculation of $t_{D_{C1}}(T)$ and $t_{D_{C2}}(T)$ are presented in Figure 7b. The comparison of parts a and b of Figure 7 shows that the diffusion times are a factor of ∼60 and ∼300 larger than the equilibration time. Since the diameter of the H_2O molecule is larger than that of HCl, the diffusion time of H_2O through the coating may be larger than that presented in Figure 7b. The large diffusion time implies that the concentration of the outer side of the coating may be only slightly larger than the equilibrium concentration of the freezing droplets.

The concentration difference can also be estimated by the comparison of the diffusion coefficients for H_2O in the 38 wt % H_2SO_4 solution and air. At $T = 188$ K, the values of the two diffusion coefficients of 38 wt % H_2SO_4 are $D_{C_1} = 4.14 \times 10^{-13}$ m²/s and $D_{C_2} = 8.30 \times 10^{-14}$ m²/s (see Figure 10). Here we assumed that the diffusion coefficients of D_{C_1} and D_{C_2} for HCl and H_2O are similar (see the previous paragraph). At the UT pressure of 200 mbar and $T = 188$ K, the diffusion coefficient in air is much larger, $D_{200} = 2.86 \times 10^{-5}$ m²/s. The very large difference between the diffusion coefficients of the solution and air is accounted for by the different densities and the very large viscosity of the 38 wt % H_2SO_4 solution (Figure 9). Further, the concentration of the outer side of the coating increases if H_2O diffuses a distance of about one monolayer (∼0.3 nm) deep into the coating. For D_{C_1} and D_{C_2} the corresponding diffusion times are $t_{D_{C1}} = 1.08 \times 10^{-7}$ s and $t_{D_{C2}} = 5.42 \times 10^{-7}$ s, respectively. One can compare these times with the time needed for H_2O in air to diffuse a larger distance, for example, a distance equal to the mean free path, L_{mfp}, of an air molecule, to replace the H_2O diffused deep into the coating. At the UT pressure of 200 mbar and $T = 188$ K, $L_{mfp} = 1.83 \times 10^{-7}$ m and the corresponding diffusion time $t_{L_{mfp}} = 5.83 \times 10^{-10}$ s. It is seen that this time is much smaller than $t_{D_{C1}}$ and $t_{D_{C2}}$. Thus, the very large difference between the diffusion coefficients of D_{C_1}, D_{C_2}, and D_{200} and, consequently, the large difference between the diffusion times in air and the coating indicate that the concentration of the outer side of the coating can be only slightly larger that the equilibrium concentration of the freezing droplets. Figure 8 shows that if the concentration difference is 0.05 wt %, the growth of the coated ice crystal to diameter 10 μm would take several days at 188 K. For the sake of comparison, the growth of the pure ice crystal to the same size would take ∼1 min. This time is similar to that (∼1 min) which is needed to consume the ice supersaturation due to vapor deposition on pure (uncoated) cirrus ice crystals.[21] The slow growth rate of the coated ice crystals slowly depletes the environmental water vapor, which can be a reason for the persistence of large in-cloud RH_i.

In the Introduction, we mentioned work which aimed to account for the large in-cloud RH_i using a deposition coefficient[22,23,26] of H_2O smaller than 0.01−0.03 in the model simulations of cirrus ice clouds. However, the physical reason for the small deposition coefficient was unclear. Our experiments suggest that, after the homogeneous freezing of aqueous aerosol droplets, the formed cirrus ice crystals will be enveloped by a residual solution coating. Therefore, in the case of the coated ice crystals one cannot speak about the deposition coefficient of H_2O. The existence of a solution coating, the concentration on the outer side of which is close to the equilibrium concentration of freezing droplets, strongly reduces the flux of H_2O condensed on the coating in comparison with the flux of H_2O deposited onto pure ice crystals. In our calculations, we assume the accommodation coefficient of condensing H_2O to be 1. However, the ratio of the fluxes of H_2O onto the coating and the pure ice surface is smaller than 0.01, i.e., similar to the small deposition coefficient which was assumed in the model simulation of cirrus ice clouds to account for the large in-cloud RH_i.

4. Conclusions

In this paper, we present experimental and computational results which demonstrate that H^+, SO_4^{2-}, and NO_3^- ions can be responsible for the buildup of clear-sky $RH_i \gg 100\%$ prior to the formation of cirrus ice clouds by homogeneous freezing of aqueous droplets containing H_2SO_4 and HNO_3. We also present the physical mechanism which can account for the observed persistent $RH_i \gg 100\%$ in cirrus ice clouds. To this end we use DSC for the study of the low-temperature phase transitions of emulsified micrometer-scaled H_2SO_4/H_2O and $H_2SO_4/HNO_3/H_2O$ droplets of sizes and compositions representative of the UT. Using the measured freezing temperatures of ice, T_i, and the thermodynamic model of the system $H^+-NH_4^+-SO_4^{2-}-NO_3^--H_2O$,[39] we calculate that the clear-sky RH_i can reach 176% prior to the formation of ice cirrus by homogeneous freezing of H_2SO_4/H_2O and $H_2SO_4/HNO_3/H_2O$ droplets. Although the value of 176% is ∼25% smaller than the largest $RH_i \approx 200\%$, which has been recently observed outside and inside the UT cirrus ice clouds,[1] it is nevertheless ∼10% larger than RH_i predicted by previous laboratory work.[9]

Our DSC measurements of H_2SO_4/H_2O and $H_2SO_4/HNO_3/H_2O$ droplets show that two endothermic-freezing and two exothermic-melting events always appear during the cooling and warming of the droplets at atmospheric temperature above ∼185 K. The warm endothermic and exothermic events consist of one transition and are due to the freezing and melting of pure ice. The cold endothermic and exothermic events, which consist of two transitions, are due to the freezing and melting of a residual solution which is formed by expelling H^+, SO_4^{2-}, and NO_3^- ions from the ice lattice. The two transitions are due to the crystallization and melting of two solids: SAO and eutectic ice/SAT.[35] Since the residual solution freezes below 185 K, the measurements suggest that if cirrus ice clouds are formed by the homogeneous freezing of aerosol droplets with a composition similar to that of laboratory droplets, then they can be composed of mixed-phase particles: a pure ice core + a residual solution

coating. Using this result, we calculate the rate of the growth of coated ice crystals and compare it with the growth rate of uncoated ice. We find that the coating may serve as a shield, slowing the rate of ice growth by $\sim 10^3$ in comparison with uncoated ice, and this can be a reason for the persistence of $RH_i \gg 100\%$ in cirrus ice clouds.

The existence of the coating around cold cirrus ice crystals may have several climatic implications: (i) The sedimentation of the small coated ice crystals is slow, and therefore, the dehydration of the UT is small. The slow growth rate of the coated ice crystals and the small dehydration prolong the lifetime of water vapor in the UT, which may contribute to the greenhouse warming because water vapor is the dominant greenhouse gas. (ii) The reduced dehydration of the UT may have an impact on the stratospheric water budget[48] and consequently on the formation of polar stratospheric clouds (PSCs) and polar ozone destruction. (iii) The coating may also change the radiative properties of cold cirrus[49] and consequently the radiative feedback mechanisms. Since the frequency of occurrence of cold cirrus clouds is large and the clouds are globally widespread,[50] the combined effect of these factors on the climate can be noticeable and, therefore, should be taken into account in global climate models.

Acknowledgment. We thank M. B. McElroy, S. C. Wofsy, E. Bertel, and T. Loerting for discussions that greatly improved the paper. A.B. thanks E. Kaija and S. Lemettinen for assistance during the performance of DSC measurements and C. Praxmarer and W. Stadlmayr for technical support.

References and Notes

(1) Krämer, M.; Schiller, C.; Afchine, A.; Bauer, R.; Gensch, I.; Mangold, A.; Schlicht, S.; Spelten, N.; Sitnikov, N.; Borrmann, S.; de Reus, M.; Spichtinger, P. *Atmos. Chem. Phys.* **2009**, *9*, 3505.

(2) Lawson, R. P.; Pilson, B.; Baker, B.; Mo, Q.; Jensen, E.; Pfister, L.; Bui, P. *Atmos. Chem. Phys.* **2008**, *8*, 1609.

(3) Jensen, E. J.; Pfister, L.; Bui, T. V.; Lawson, P.; Baker, B.; Mo, Q.; Baumgardner, D.; Weinstock, E. M.; Smith, J. B.; Moyer, E. J.; Hanisco, T. F.; Sayres, D. S.; Clair, J. M. St.; Alexander, M. J.; Toon, O. B.; Smith, J. A. *Atmos. Chem. Phys.* **2008**, *8*, 1621.

(4) Gao, R. S.; Popp, P. J.; Fahey, D. W.; Marcy, T. P.; Herman, R. L.; Weinstock, E. M.; Baumgardner, D.; Garrett, T. J.; Rosenlof, K. H.; Thompson, T. L.; Bui, P. T.; Ridley, B. A.; Wofsy, S. C.; Toon, O. B.; Tolbert, M. A.; Kärcher, B.; Peter, Th.; Hudson, P. K.; Weinheimer, A. J.; Heymsfield, A. J. *Science* **2004**, *303*, 516.

(5) Khvorostyanov, V. I.; Curry, J. A. *J. Geophys. Res.* **2009**, *114*, D04207.

(6) Angell, C. A. Supercooled Water. In *Water: A Comprehensive Treatise*; Franks, F., Ed.; Plenum Press: New York and London, 1982; Vol. 7, Chapter 1.

(7) Mishima, O.; Stanley, H. E. *Nature* **1998**, *396*, 329.

(8) Bogdan, A.; Molina, M. J.; Sassen, K.; Kulmala, M. *J. Phys. Chem A* **2006**, *110*, 12541.

(9) Koop, T.; Ng, H. P.; Molina, L. T.; Molina, M. J. *J. Phys. Chem. A* **1998**, *102*, 8924.

(10) Yamato, M.; Ono, A. *J. Meteorol. Soc. Jpn.* **1989**, *67*, 147.

(11) McCormick, M. P.; Thomason, L. W.; Trepte, C. R. *Nature* **1995**, *373*, 399.

(12) Capaldo, K.; Corbett, J. J.; Kasibhatla, P.; Fischbeck, P.; Pandis, S. N. *Nature* **1999**, *400*, 743.

(13) Duce, R. A.; LaRoche, J.; Altieri, K.; Arrigo, K. R.; Baker, A. R.; Capone, D. G.; Cornell, S.; Dentener, F.; Galloway, J.; Ganeshram, R. S.; Geiger, R. J.; Jickells, T.; Kuypers, M. M.; Langlois, R.; Liss, P. S.; Liu, S. M.; Middelburg, J. J.; Moore, C. M.; Nickovic, S.; Oschlies, A.; Pedersen, T.; Prospero, J.; Schlitzer, R.; Seitzinger, S.; Sorensen, L. L.; Uematsu, M.; Ulloa, O.; Voss, M.; Ward, B.; Zamora, L. *Science* **2008**, *320*, 893.

(14) Dentener, F. J.; Crutzen, P. J. *J. Atmos. Chem.* **1994**, *19*, 331.

(15) Sassen, K.; Dodd, G. C. *J. Atmos. Sci.* **1988**, *45*, 1357.

(16) Khvorostyanov, V. I.; Sassen, K. *Geophys. Res. Lett.* **1998**, *25*, 3155.

(17) Khvorostyanov, V. I.; Morrison, H.; Curry, J. A.; Baumgardner, D.; Lawson, P. *J. Geophys. Res.* **2006**, *111*, D02201, DOI: 10.1029/2004JD005235.

(18) Bertram, A. K.; Koop, T.; Molina, L. T.; Molina, M. J. *J. Phys. Chem. A* **2000**, *104*, 584.

(19) DeMott, P. J.; Cziczo, D. J.; Prenni, A. J.; Murphy, D. M.; Kreidenweis, S. M.; Thomson, D. S.; Borys, R.; Rogers, D. S. *Proc. Natl. Acad. Sci. U.S.A.* **2003**, *100*, 14–655.

(20) Tompkins, A. M.; Gierens, K.; Rädel, G. Q. J. R. *Meteorol. Soc.* **2007**, *133*, 53.

(21) Peter, T.; Marcolli, K.; Spichtinger, P.; Corti, T.; Baker, M. B.; Koop, T. *Science* **2006**, *314*, 1399.

(22) Khvorostyanov, V. I.; Sassen, K. *J. Atmos. Sci.* **1998**, *55*, 1822.

(23) Gierens, K. M.; Monier, M.; Gayet, J.-F. *J. Geophys. Res.* **2003**, *108* (D2), 4069.

(24) Haag, W.; Kärcher, B.; Schaefers, S.; Stetzer, O.; Möhler, O.; Schurath, U.; Krämer, M.; Schiller, C. *Atmos. Chem. Phys.* **2003**, *8*, 195.

(25) Magee, N.; Moyle, A. M.; Lamb, D. *Geophys. Res. Lett.* **2006**, *33*, L17813.

(26) Lin, R.-F.; Starr, D. O'C.; DeMott, P. J.; Cotton, R.; Sassen, K.; Jensen, E.; Kärcher, B.; Liu, X. *J. Atmos. Sci.* **2002**, *59*, 2305.

(27) McGraw, R. *Science* **2004**, *304*, 961.

(28) Shilling, J. E.; Tolbert, M. A.; Toon, O. B.; Jensen, E. J.; Murray, B. J.; Bertram, A. K. *Geophys. Res. Lett.* **2006**, *33*, L17801.

(29) Bogdan, A.; Loerting, T. *EGU Gen. Assem.* **2009**, *11*, EGU2009-13419.

(30) Chang, H.-Y. A.; Koop, T.; Molina, L. T.; Molina, M. J. *J. Phys. Chem.* **1999**, *103*, 2673.

(31) Carslaw, K. S.; Wirth, M.; Tsias, A.; Luo, B. P.; Dörnbrack, A.; Leutbecher, M.; Volkert, H.; Renger, W.; Bacmeister, J. T.; Peter, T. *J. Geophys. Res.* **1998**, *103*, 5785.

(32) Luo, B. P.; Peter, T.; Wernli, H.; Fueglistaler, S.; Wirth, M.; Kiemle, C.; Flentje, H.; Yushkov, V. A.; Khattanov, V.; Rudakov, V.; Thomas, A.; Borrmann, S.; Toci, G.; Mazzinghi, P.; Beuermann, J.; Schiller, C.; Cairo, F.; Di Don-Francesco, G.; Adriani, A.; Volk, C. M.; Strom, J.; Noone, K.; Mitev, V.; MacKenzie, R. A.; Carslaw, K. S.; Trautmann, T.; Santacesaria, V.; Stefanutti, L. *Atmos. Chem. Phys.* **2003**, *3*, 1093.

(33) Bogdan, A. *J. Phys. Chem. B* **2006**, *110*, 12205.

(34) Gable, C. M.; Betz, H. F.; Maron, S. H. *J. Am. Chem. Soc.* **1950**, *72*, 1445.

(35) Beyer, K. D.; Hansen, A. R.; Poston, M. *J. Phys. Chem. A* **2003**, *107*, 2025.

(36) Beyer, K. D.; Hansen, A. R.; Raddatz, N. *J. Phys. Chem. A* **2004**, *108*, 770.

(37) Beyer, K. D.; Hansen, A. R. N. *J. Phys. Chem. A* **2002**, *106*, 10275.

(38) Curry, J. A.; Webster, P. J. *Thermodynamics of Atmospheres and Oceans*; Academic Press: New York, 1999; Vol. 65.

(39) Clegg, S. L.; Brimblecombe, P.; Wexler, A. S. *J. Phys. Chem. A* **1998**, *102*, 2137.

(40) Nousiainen, T.; McFarquhar, G. M. *J. Atmos. Sci.* **2004**, *61*, 2229.

(41) Kauffeld M. *Handbook on Ice Slurries: Fundamentals and Engineering*; International Institute of Refrigeration: Paris, 2005.

(42) Thomas, A.; Borrmann, S.; Kiemle, C.; Cairo, F.; Volk, M.; Beuermann, J.; Lepuchov, B.; Santacesaria, V.; Matthey, R.; Rudakov, V.; Yushkov, V.; MacKenzie, A. R.; Stefanutti, L. *J. Geophys. Res.* **2002**, *107* (0), DOI: 10.1029/2001JD001385.

(43) Steele, H. M.; Hamill, P. *J. Aerosol. Sci.* **1981**, *12*, 517.

(44) Williams, L. R.; Golden, D. M. *Geophys. Res. Lett.* **1993**, *20*, 2227.

(45) Pruppacher, H. R.; Klett, J. D. *Microphysics of Clouds and Precipitation*; Kluwer: Dordrecht, The Netherlands, 1997.

(46) Wagner, P. E. Aerosol Growth and Condensation. In *Aerosol Microphysics, Vol. II, Chemical Physics of Microparticles*; Marlow, W. H., Ed.; Springer-Verlag: New York, 1982; Chapter 5.

(47) Williams, L. R.; Long, F. S. *J. Phys. Chem.* **1995**, *99*, 3748.

(48) Rosenfield, J. E.; Considine, D. B.; Schoeberl, M. R.; Browell, E. V. *Geophys. Res. Lett.* **1998**, *25*, 1883.

(49) Räisänen, P.; Bogdan, A.; Sassen, K.; Kulmala, M.; Molina, M. J. *Atmos. Chem. Phys.* **2006**, *6*, 4659.

(50) Winker, D. M.; Trepte, C. R. *Geophys. Res. Lett.* **1998**, *25*, 3351.

JP9063609